Electronic Supplementary Material (ESI) for Journal of Materials Chemistry A.
This journal is © The Royal Society of Chemistry 2024

Supporting Information

Constructing $FeSe_2$ nanorods supported on ketjenblack with superior cyclability for potassium-ion batteries

Bi-Cui Chen[1], Xian Lu[1], Hou-Yang Zhong[1], Pei-Weng Huang[1], Ya-Nan Wu[1], Si-Yu Xu[1], Xue-You Tan[2,] and Xiao-Hui Wu[1,*]*

1 College of Chemistry and Materials Science, Fujian Provincial Key Laboratory of Advanced Materials Oriented Chemical Engineering, Fujian Normal University, Fuzhou 350007, China. E-mail: sherrywu@fjnu.edu.cn

2 Guangxi Key Laboratory of Automobile Components and Vehicle Technology, School of Mechanical and Automotive Engineering, Guangxi University of Science and Technology, Liuzhou, 545006, P. R. China. E-mail: tanxueyou123@163.com

Experiments

Chemicals and Materials

Ferrocene ($Fe(C_5H_5)_2$, 99%), selenium powder (99.99%), and perylene-3,4,9,10-tetracarboxylic dianhydride (PTCDA, 98%) were brought from Adamas. Red phosphorus powder (97.00%) was purchased from Acros. Ketjen black (KB) and carboxy methyl cellulose sodium (NaCMC, 99%) were obtained from Canrd. Poly(vinylidene difluoride) (PVDF, 99.5%) was purchased from SOLVAY. N, N-dimethylformamide (DMF, 99.5%) was purchased from Greagent. All the above reagents were used directly without additional treatment.

Materials Synthesis

Synthesis of $FeSe_2$@C-x (x=0, 1, 3, 5) and FeP@C-3

Taking the synthesis of $FeSe_2$@C-3 as an example: 100 mg ferrocene (0.5 mmol), 160 mg selenium powder (2.0 mmol), and 30 mg carbon black were mixed evenly. The mixture was transferred to a quartz tube which was evacuated using an oil pump and then sealed. The vacuum-sealed quartz tube was placed in a double-temperature zone tube furnace for high-temperature selenization. After preheating at 110℃ for 10 minutes, the temperature of the sample end was set to 450℃ and the non-sample end to 300℃ for 30 minutes. After the quartz tube cools to room temperature, $FeSe_2$@C-3 could be obtained. Under the condition that other preparation conditions remain unchanged, the addition of raw materials for different samples was listed in the following table:

Sample	Ferrocene (mg)	Selenium (mg)	Red phosphorus (mg)	KB (mg)
$FeSe_2$@C-0	100	160	0	0
$FeSe_2$@C-1	100	160	0	10
$FeSe_2$@C-3	100	160	0	30
$FeSe_2$@C-5	100	160	0	50
FeP@C-3	100	0	60	30

Materials Characterization

The crystalline phases of the as-prepared samples were characterized via the powder X-ray diffractometer (PXRD, Bruker D8 Advance) with Cu Kα radiation (λ = 1.5418 Å). The structure and composition of the as-prepared samples were characterized by scanning electron microscopy (SEM, Hitachi SU8100), regular transmission electron microscopy (TEM, JEOL 2100F), and high-resolution transmission electron microscope (HRTEM) including high-angle annular dark-field scanning transmission electron microscope (HAADF-STEM) equipped with associated the energy dispersive X-ray spectroscopy (EDS). The chemical compositions and the bonding structures were determined by X-ray photoelectron spectroscopy (XPS) spectra (Thermo ESCALAB 250XI). Raman spectra were obtained by using a Micro-Raman spectroscopy system (LabRAM HR Evolution) under a laser excitation of 532 nm wavelength. The specific surface area was measured with a BELSORP-Mini II instrument. Thermal gravimetric analysis (TGA NETZSCH STA 449F3) was performed up to 800°C at a heating rate of 10°C/min in the air atmosphere.

Electrochemical Measurements

1. Half Cells

The electrochemical properties of samples were measured using coin cells (CR2032). The electrodes were obtained via the following method: 40 mg samples, 5 mg KB, and 5 mg PVDF (8: 1: 1) were dispersed in NMP to form a slurry under continuous stirring. Subsequently, the slurry was smeared on copper foil uniformly, and dried at 80^{o}C for 12 h. The loading of the active materials was ensured at approximately 0.8-1.2 mg cm^{-2}. The fabricated electrode was used to construct the half-cells in an Ar-filled glove box. The half cells were assembled by using the synthesized $FeSe_2$@C-x (x=0, 1, 3, 5), FeP@C-3 or PTCDA electrodes as the working electrodes, potassium as the reference electrode, Whatman GF/D glass fiber as the separator and 1.0 M KFSI solution in a mixture of Ethylene Carbonate and Diethyl Carbonate (1: 1 in volume) as the electrolyte. The voltage range for the PTCDA-based half cells was 1.5-3.5 V but 0.005-2.8 V for the other half cells. The galvanostatic charge/discharge tests were carried out

at 30°C using a LAND cycler test system. Both cyclic voltammetry (CV) and electrochemical impedance spectroscopy (EIS) were performed with a CHI660d electrochemistry workstation (CH instrument, Shanghai).

2. Full Cells

The preparation was similar to the half cells. In a full cell, the $FeSe_2$@C-3 electrode was used as the anode and the PTCDA electrode was applied as the cathode. Before assembling the full cells, the PTCDA cathodes were pre-cycled in half-cells at 0.1 A g^{-1} between 1.5 and 3.5 V for three turns, and the $FeSe_2$@C-3 anode was cycled in half-cells for two cycles over a potential range of 0.005 to 2.8 V and then discharged to 0.005 V at 0.1 A g^{-1}. The voltage range for the full cells was 0.5-3.4 V.

Theoretical Calculations

To explore the effect of the structure of $FeSe_2$ and FeP on potassiation process, the first principles calculation based on the density functional theory (DFT) was carried out at the atomic level. The K^+ adsorption energy on the $FeSe_2$ and FeP were calculated in DMol^3 code.[1] The molecular dynamics (MD) simulations were performed based on the density functional theory (DFT) using the Forcite module.

1. The construction of three models: A supercell of $FeSe_2$ (2×2×1) with the parameters of a=9.608 Å, b=11.568 Å, c= 3.586 Å, α= β= γ= 90^o was built as sc- $FeSe_2$ model; A supercell of FeP (2×1×1) with the parameters of a=10.386 Å, b=6.198 Å, c= 5.792 Å, α= β= γ= 90^o was built as sc-FeP model. The chemical formula of sc- $FeSe_2$ and sc-FeP is Fe_8Se_{16} and Fe_8P_8, respectively. The geometry optimization process employed the Perdew-Burke-Eznerhof (PBE) with generalized gradient approximation (GGA) for the exchange-correlation functional.[2] The basis-set was double numerical orbital base group and orbital polarization function (DNP) and the basis file was set to be 3.5. The Grimme scheme was included for the dispersion correction.[3] During the coordinate's relaxation, the convergence criteria for the geometry optimization were set to 2.0 × 10 $^{-5}$ Ha for energy, 0.004 Ha Å^{-1} for force, and 0.005 Å for displacement. The self-consistent field convergence for the single point energy calculation was set to 1.0 × 10^{-5} Ha, and global orbital cutoff is 5.0 Å. The Monkhorst-Pack k-point mesh was

0.04 1/Å.

2. The calculation of K^+ intercalation energy: The K^+ intercalation energies (E_{in}) of sc-$FeSe_2$ and sc-FeP models were calculated as follows:

$E_{in} = E_{composite} - E_{pristine} - E_K$

where $E_{composite}$ was the total energy of the sc- $FeSe_2$ and sc-FeP after K intercalation, $E_{pristine}$ was the total energy of geometry-optimized sc- $FeSe_2$ and sc-FeP, and E_K is the chemical potential of K atom.

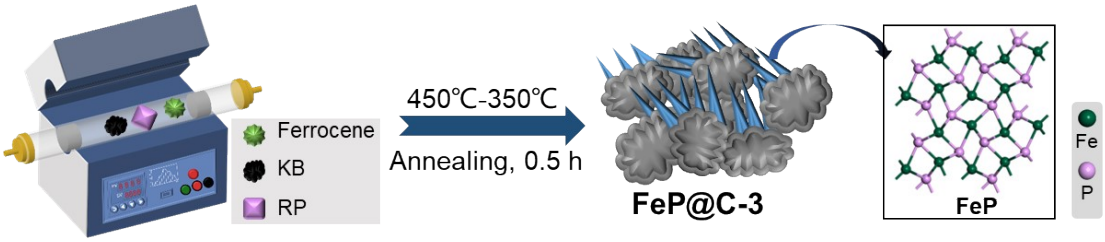

Figure S1. Scheme of the synthesis process for FeP@C-3 sample.

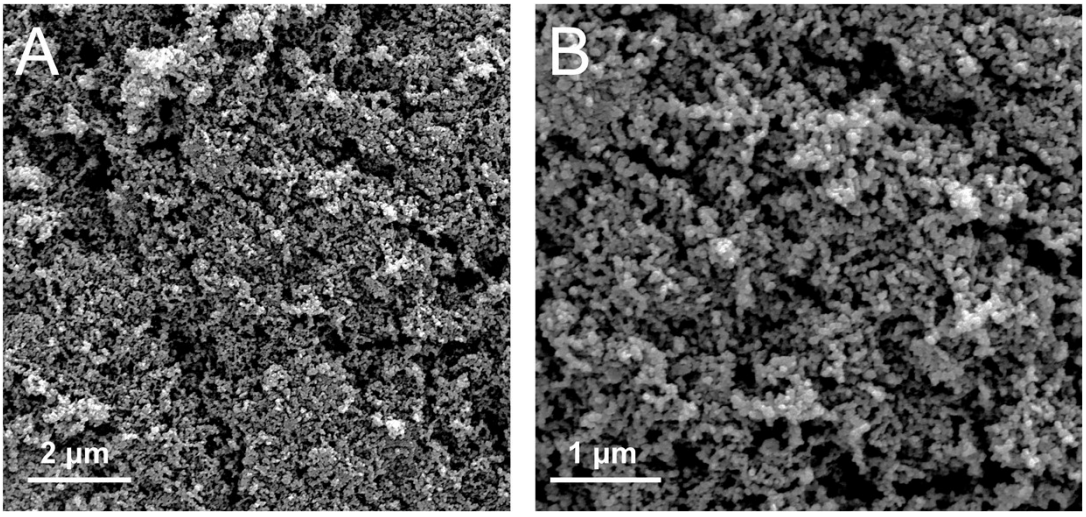

Figure S2. SEM images of KB carbon at different magnifications.

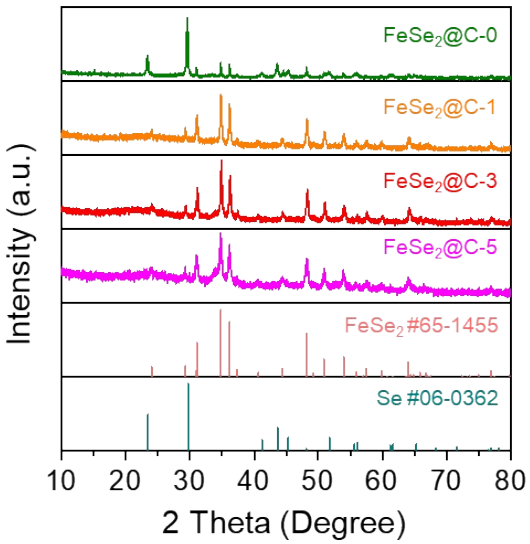

Figure S3. PXRD patterns of $FeSe_2$@C-0, $FeSe_2$@C-1, $FeSe_2$@C-3, and $FeSe_2$@C-5 samples along with the corresponding standard patterns of $FeSe_2$ and Se.

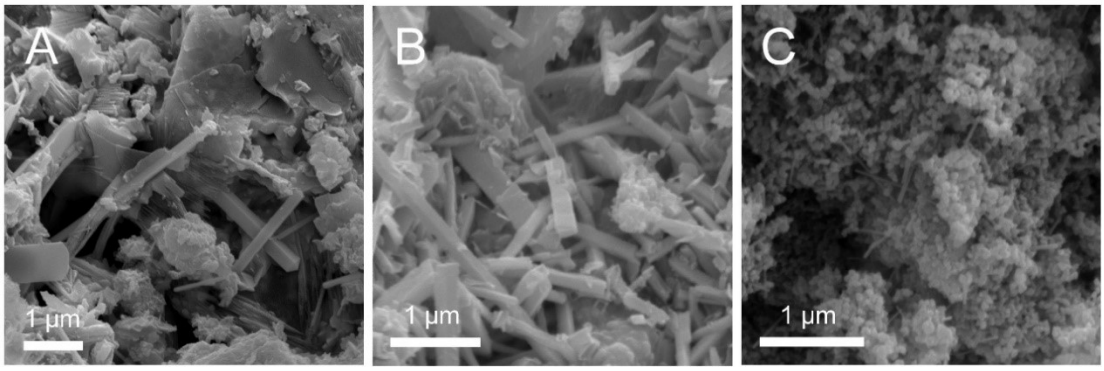

Figure S4. SEM images of (A) $FeSe_2$@C-0, (B) $FeSe_2$@C-1, and (C) $FeSe_2$@C-5.

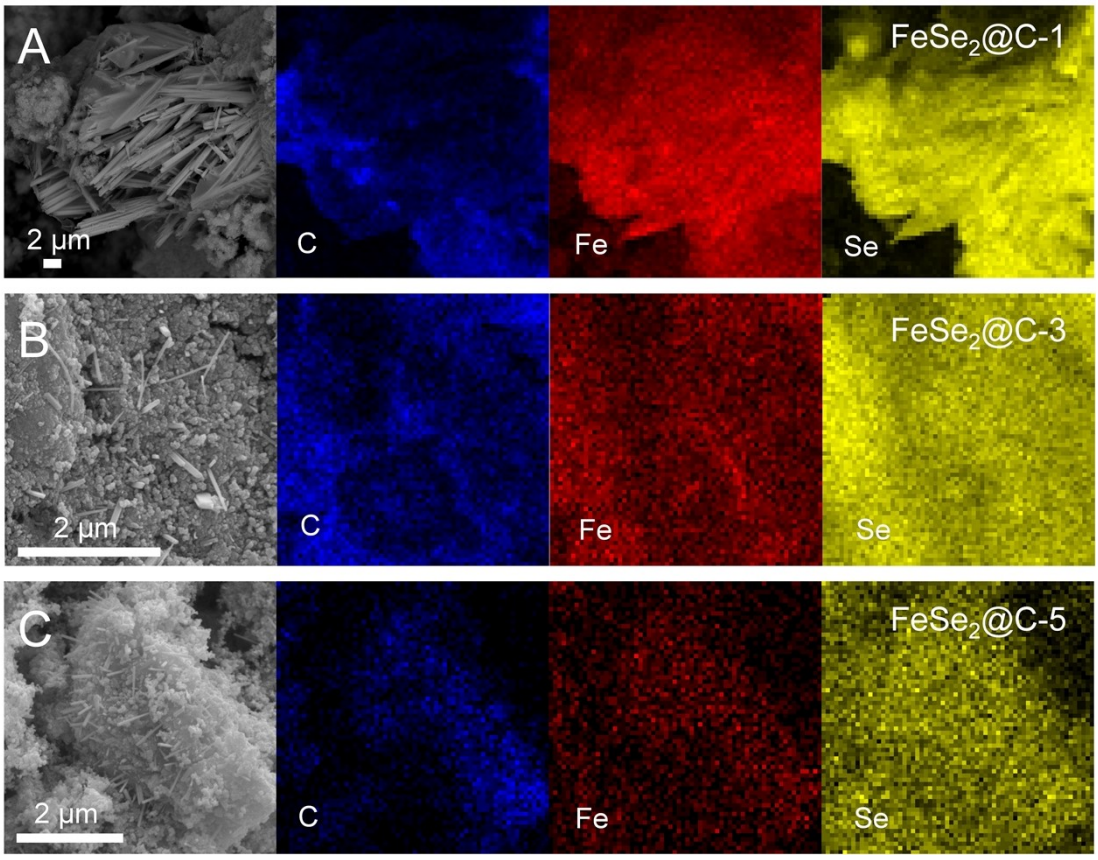

Figure S5. The element mapping of (A) $FeSe_2$@C-1, (B) $FeSe_2$@C-3, and (C) $FeSe_2$@C-5.

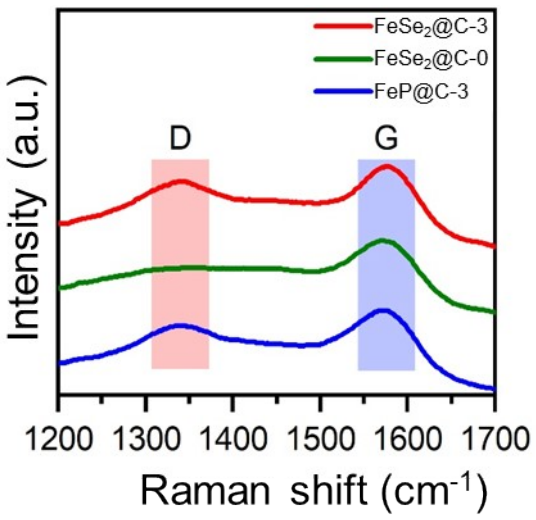

Figure S6. Raman spectra of $FeSe_2$@C-3, $FeSe_2$@C-0 and FeP@C-3 in the range of 1200-1700 cm^{-1}

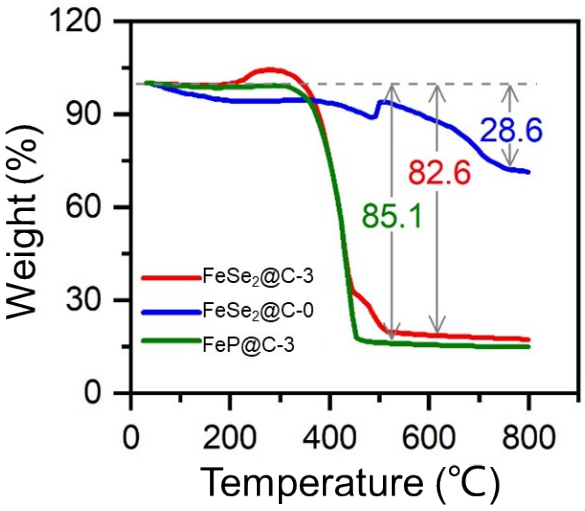

Figure S7. TG analysis curves of $FeSe_2$@C-3, FeP@C-3, and $FeSe_2$@C-0 in air atmosphere from 30-800℃.

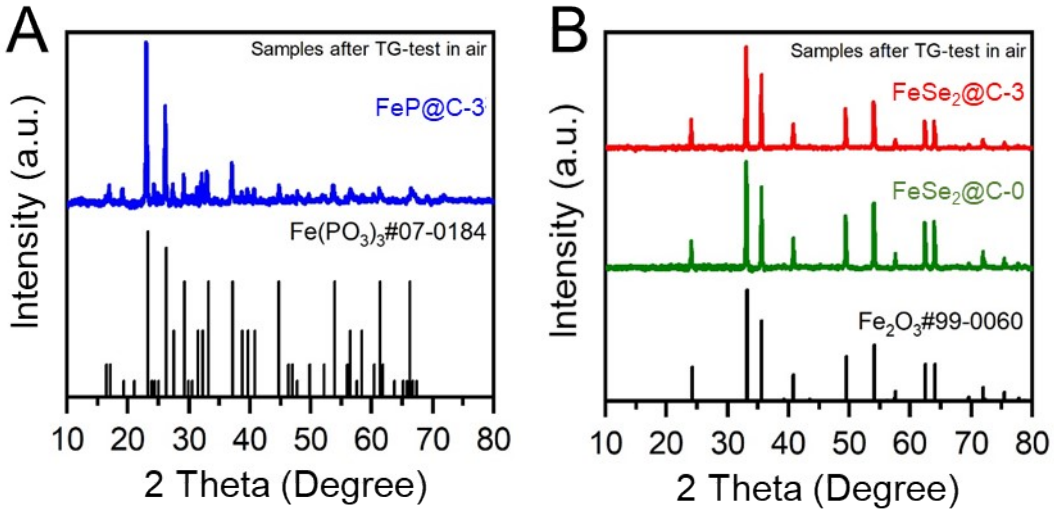

Figure S8. PXRD patterns of annealed (A) FeP@C-3, (B) $FeSe_2$@C-3, and $FeSe_2$@C-0 samples after TG test in air atmosphere from 30-800℃.

The calculation process:

Based on the above results, let x represent the mass percentage of $FeSe_2$ in $FeSe_2$@C-3, and let y represent the mass percentage of FeP in FeP@C-3. The following equation is used for calculation:

$$(100\% - 82.6\%) * \frac{56 * 2}{56 * 2 + 16 * 3} = x * \frac{56}{56 + 79 * 2} \quad (1)$$

$$(100\% - 28.6\%) * \frac{56}{56 + (31 + 16 * 3) * 3} = y * \frac{56}{56 + 31} \quad (2)$$

By calculation, the mass percentage of $FeSe_2$ in $FeSe_2$@C-3 material is 46.5%, and the mass percentage of FeP in FeP@C-3 material is 21.2%. Further calculation reveals that the atomic percentage of $FeSe_2$ in $FeSe_2$@C-3 material is 4.5%, and the atomic percentage of FeP in FeP@C-3 material is 3.6%.

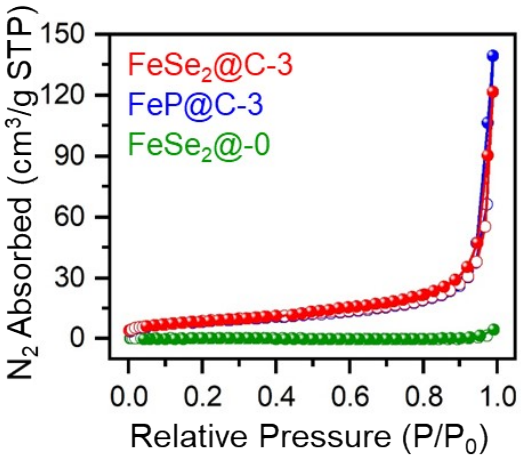

Figure S9. N_2 adsorption-desorption isotherms of $FeSe_2$@C-3, FeP@C-3 and $FeSe_2$@C-0.

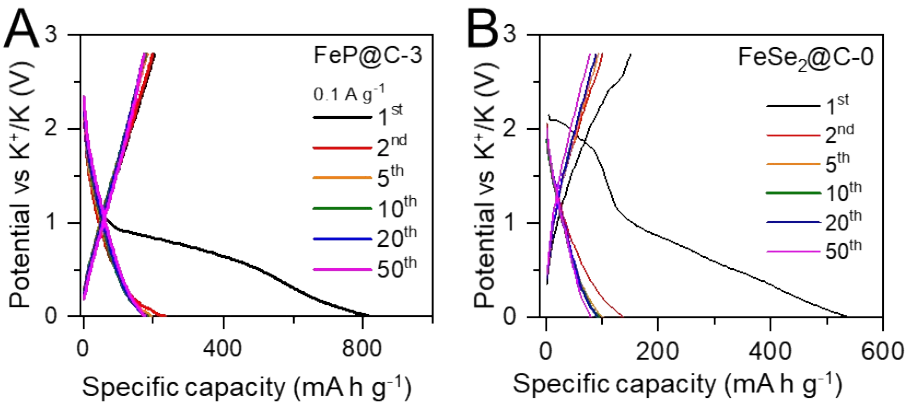

Figure S10. The discharge-charge curves of (A) FeP@C-3 and (B) $FeSe_2$@C-0 electrode at different cycles at 0.1 A g^{-1}.

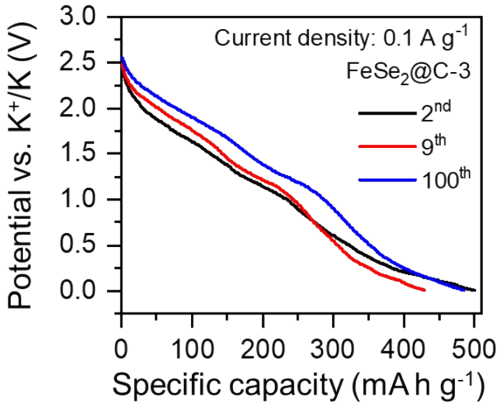

Figure S11. The galvanostatic discharge profiles of $FeSe_2$@C-3 at the 2nd, 9th, and 100th cycles at 0.1 A g^{-1}.

Table S1. The specific capacity increments of $FeSe_2$@C-3 electrode in three voltage ranges.

Voltage range (V)	Specific capacity (mA h g^{-1})				
	2^{nd}	9^{th}	100^{th}	$\triangle C_{9-2}$	$\triangle C_{100-9}$
0.5-0.005	175	122	133	-53	11
1.5-0.5	196	164	174	-32	10
2.6-1.5	126	141	176	15	35
Full range	497	427	483	-70	56

Table S2. Comparison of the cycling performance of $FeSe_2$@C-3 and other $FeSe_2$-based materials for PIBs anodes.

Material	**Current density (A g^{-1})**	**Cycle number**	**Specific capacity (mA h g^{-1})**	**Ref.**
$FeSe_2$@C-3	0.1	100	486	This work
	1.0	3500	286	
NFS@NC@C	5.0	1200	107.7	4
$FeSe_2$/NC	1.0	250	301	5
$FeSe_2$@NC	2.0	5000	24.1	6
$FeSe_2$/N-C	2.0	2000	158	7
$FeSe_2$@C NBs	0.1	700	221	8

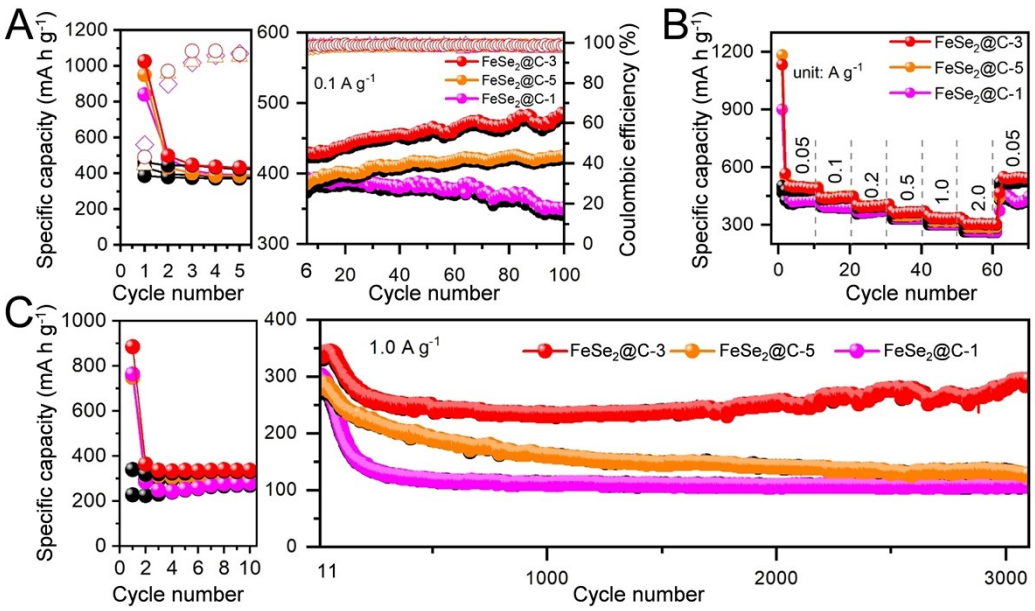

Figure S12. (A) The cycling performance at a current density of 0.1 A g^{-1}, (B) rate performance at various current densities, and (C) long-term cyclic performance at 1.0 A g^{-1} of $FeSe_2$@C-3, $FeSe_2$@C-1 and $FeSe_2$@C-5 electrodes.

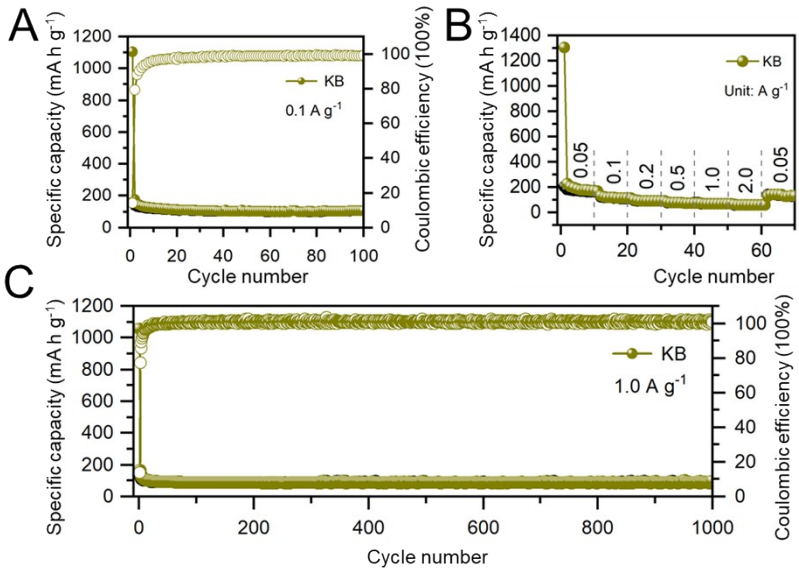

Figure S13. (A) Cycling performance, (B) rate performance and (C) long-term cyclic performance of the KB electrode.

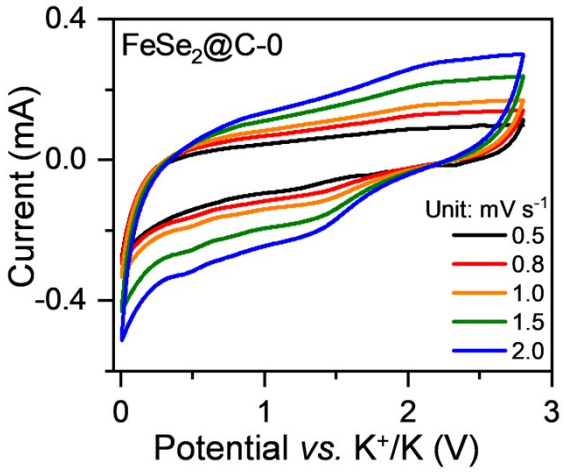

Figure S14. CV curves of $FeSe_2$@C-0 electrode at different scan rates from 0.5 to 2.0 mV s^{-1}.

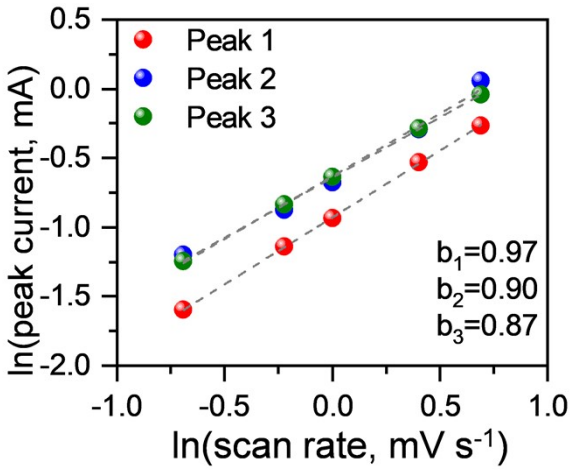

Figure S15. The ln(i) versus ln(v) plot of the peak current of $FeSe_2$@C-3.

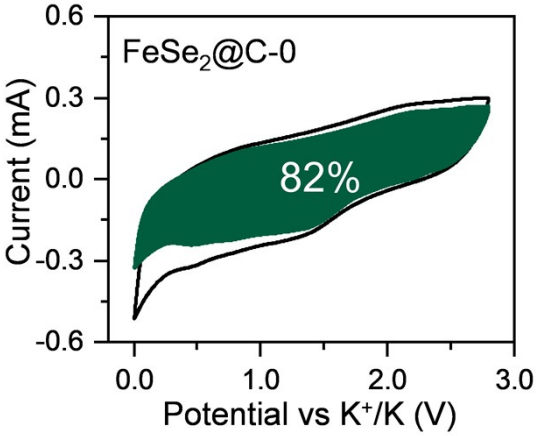

Figure S16. The capacitive charge storage contribution to the charge storage at 0.5 mV s^{-1} for the $FeSe_2$@C-0 electrode.

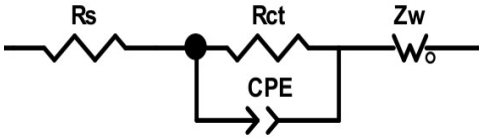

Figure S17. The equivalent circuit for the EIS spectra of the $FeSe_2$@C-3, FeP@C-3, and $FeSe_2$@C-0 electrodes.

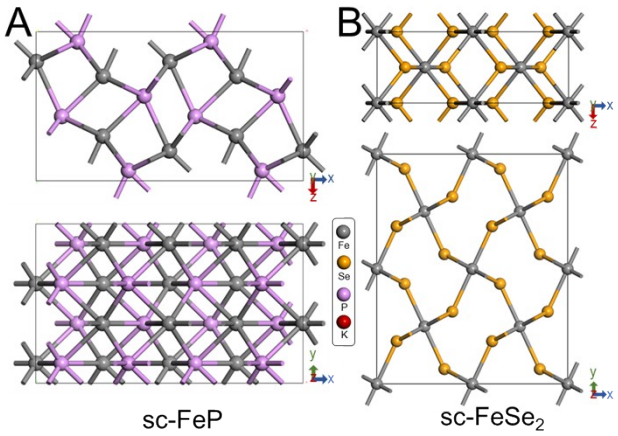

Figure S18. The constructed models of (A) sc-FeP and (B) sc-$FeSe_2$.

References

1. Delley, B., From molecules to solids with the DMol3 approach. *The Journal of Chemical Physics* **2000,** *113* (18), 7756-7764.
2. Perdew, J. P.; Burke, K.; Ernzerhof, M., Generalized gradient approximation made simple. *Physical Review Letters* **1996,** *77* (18), 3865.
3. Grimme, S.; Antony, J.; Ehrlich, S.; Krieg, H., A consistent and accurate ab initio parametrization of density functional dispersion correction (DFT-D) for the 94 elements H-Pu. *The Journal of Chemical Physics* **2010,** *132* (15), 154104.
4. Gong, J.; Zhang, R.; Wei, X.; Liu, Y.; Luo, Q.; Wan, Q.; Zheng, Q.; Wang, L.; Liu, S.; Lin, D., Spatially dual-confined metallic selenide double active centers for boosting potassium ion storage. *Chemical Engineering Journal* **2023,** *459*, 141609.
5. Liu, Y. Z.; Yang, C. H.; Li, Y. P.; Zheng, F. H.; Li, Y. J.; Deng, Q.; Zhong, W. T.; Wang,

G.; Liu, T. Z., $FeSe_2$/nitrogen-doped carbon as anode material for Potassium-ion batteries. *Chemical Engineering Journal* **2020,** *393*, 124590.

6. Wu, H.; Lu, S.; Xu, S.; Zhao, J.; Wang, Y.; Huang, C.; Abdelkader, A.; Wang, W. A.; Xi, K.; Guo, Y.; Ding, S.; Gao, G.; Kumar, R. V., Blowing Iron Chalcogenides into Two-Dimensional Flaky Hybrids with Superior Cyclability and Rate Capability for Potassium-Ion Batteries. *ACS Nano* **2021,** *15* (2), 2506-2519.
7. Ge, J. M.; Wang, B.; Wang, J.; Zhang, Q. F.; Lu, B. G., Nature of $FeSe_2$/N-C Anode for High Performance Potassium Ion Hybrid Capacitor. *Advanced Energy Materials* **2020,** *10* (4), 1903277.
8. Liu, C.; Li, Y. J.; Feng, Y. H.; Zhang, S.; Lu, D.; Huang, B. Y.; Peng, T.; Sun, W. W., Engineering of yolk-shelled $FeSe_2$@nitrogen-doped carbon as advanced cathode for potassium-ion batteries. *Chinese Chemical Letters* **2021,** *32* (11), 3601-3606.